ISSN 1063-780X, Plasma Physics Reports, 2023, Vol. 49, No. 12, pp. 1542–1551. © The Author(s), 2023. This article is an open access publication.
Russian Text © The Author(s), 2023, published in Fizika Plazmy, 2023, Vol. 49, No. 12, pp. 1337–1347.

TOKAMAKS

Features of Plasma Disruption in the Globus-M2 Spherical Tokamak

N. V. Sakharov[a,*], A. A. Kavin[b], A. B. Mineev[b,**], N. N. Bakharev[a], E. N. Bondarchuk[b], V. K. Gusev[a], N. S. Zhiltsov[a], E. O. Kiselev[a], G. S. Kurskiev[a], V. B. Minaev[a], Yu. V. Petrov[a], I. Yu. Rodin[b], O. M. Skrekel[a], A. Yu. Telnova[a], E. E. Tkachenko[a], V. A. Tokarev[a], E. A. Tukhmeneva[a], and P. B. Shchegolev[a]

[a] Ioffe Institute, Russian Academy of Sciences, St. Petersburg, 194021 Russia
[b] Efremov Institute of Electrophysical Apparatus, St. Petersburg, 196641 Russia
*e-mail: nikolay.sakharov@mail.ioffe.ru
**e-mail: min-anat@mail.ru

Received September 5, 2023; revised October 26, 2023; accepted November 1, 2023

Abstract—Data on plasma disruption processes in the modernized Globus-M2 spherical tokamak are presented. Electron temperature and density profiles before the disruption, immediately after thermal quench and in the stage of plasma current quench are measured using the diagnostics of Thomson scattering of laser radiation. The dependence of the plasma current decay time during disruption on the pre-disruption current value is determined. The distribution of the toroidal current, which is induced during disruption, in the shell of the vessel is determined on the basis of magnetic measurements. Electromagnetic loads on the vessel are calculated.

Keywords: spherical tokamak, Globus-M2, thermal quench, current quench, scaling

DOI: 10.1134/S1063780X23601748

1. INTRODUCTION

In [1, 2], main disruptions in the Globus-M spherical tokamak were analyzed at a plasma current level $I_p \le 230$ kA and a toroidal magnetic field $B_{T0} \le 0.5$ T. The main differences in the obtained dependences of the current quench duration t_{CQ} from the data accumulated for the ITER project were noted [3, 4]. In accordance with the international database on disruptions, the linear current quench time is defined as $t_{CQ} = (t_{20} - t_{80})/0.6$, where t_{80}, t_{20} are times, when the plasma current reaches 80 and 20% of the initial value before the quench (the subscript CQ means current quench). Also, the international database uses the normalization of t_{CQ} to the cross-sectional area of the plasma before disruption S to compare disruption times in tokamaks of different sizes.

In [1], it was shown that a number of regularities of plasma parameters during disruptions in the Globus-M spherical tokamak differ significantly from the expected parameters of the ITER project [3, 4]. The main difference is the increase in the current quench duration t_{CQ} as the plasma current I_p increases, which is close to a linear law. Another feature noted in [1, 2] is related to the character of the input of impurities into the discharge during disruption: the best agreement between experiment and calculation data was obtained at a linear law of the impurity accumulation (in the ITER project, the main input of impurities is assumed at the thermal quench stage, which precedes current quench). Finally, the absence of runaway electrons during disruption was noted. These differences generally favor the mitigation of the consequences of disruptions in a spherical tokamak. A comparison of a number of experimental parameters of disruptions in Globus-M and Globus-M2 tokamaks (the plasma sizes in both facilities are as follows: the major radius $R = 0.36$ m, and the minor radius $a = 0.24$ m) and their expected values in the ITER project are given in Table 1.

This work is the continuation of the analysis begun for the experiments at the Globus-M tokamak using data of the Globus-M2 spherical tokamak at an increased plasma current $I_p \le 430$ kA and a toroidal magnetic field $B_{T0} \le 0.9$ T in order to find out whether regularities and trends noted in [1, 2] are traced. These issues are especially important from the point of view of extrapolating the results to the parameters of the forthcoming facility, the Globus-3 spherical tokamak [5–7] with a plasma current $I_p \sim 800$ kA and a toroidal magnetic field $B_{T0} \sim 1.5$ T, which, according to a number of indicators, can be considered as a hydrogen prototype of a neutron source.

It is important to note that the t_{CQ} value in the Globus-M2 at a plasma current I_p ~400 kA is on a scale of milliseconds and higher. In this case, the diagnostics available on the Globus-M2 allow direct measure-

Table 1. Comparison of experimental and expected disruption parameters in the Globus and ITER facilities

Characteristic	ITER Database [3, 4]	Globus-M Database [1, 2]
Ratio of thermal and current quench durations	$t_{tQ} \ll t_{CQ}$	$t_{tq} < t_{CQ}$
Average electron temperature during plasma current quench T_e, eV	≤5–10	≥10
Mechanism of physical sputtering of walls during current quench	Does not work	Works
Input of impurities into plasma during disruption	Mainly during thermal quench	During both thermal and current quench
Generation of runaway electrons	Generation is very probable	Generation is hardly probable
Scaling for the minimum duration $t_{CQ,min}$ of current quench	Scaling $t_{CQ,min}$ depends weakly on j_p (*) $t_{CQ,min}/S \approx 1.67$ ms/m^2	$t_{CQ,min}/S \propto j_p$. At $j_p > 0.5$ MA/m^2 $t_{CQ,min}/S > 1.67$ ms/m^2

(*) j_p is the current density before the quench, $j_p = I_p/S$, where S is the plasma cross-sectional area before disruption.

ments of a number of plasma characteristics (in particular, electron density and temperature profiles) directly during the current quench. Plasma is probed with laser in the Thomson scattering diagnostics during the entire discharge pulse. Laser pulses follow with a period of 3 ms.

The new database of disruptions in the Globus-M2 tokamak includes several dozen discharges with the deuterium plasma. The range of plasma parameters before the disruption is: B_{T0} = 0.6–0.91 T; I_p = 70–426 kA; the elongation of the plasma cross section in the vertical direction κ = 1.36–1.96; the triangularity δ = 0.16–0.35 (the δ value is defined as half the sum of the upper and lower triangularity); and the aspect ratio R/a = 1.58–2.08. In most discharges, one or two atomic beams with energies of up to 30 and 50 keV, respectively, were injected into the plasma. The total injection power reached 1.6 MW.

2. EXPERIMENTAL RESULTS

Figure 1 shows the parameters of the discharge 42784 typical for the collected database (the plasma current before disruption $I_p \approx 330$ kA), in which the laser pulse of the Thomson scattering diagnostics of laser radiation got into a short time interval between thermal quench and current quench (a sharp decrease in the intensity of soft X-ray radiation SXR is observed at the time of thermal quench). In the discharge 42784, a deuterium beam with an atomic energy of 30 keV and a power of 0.7 MW was injected into the deuterium plasma. The beam injection was terminated approximately 1 ms before the plasma disruption.

Electron temperature and density profiles at two times before thermal quench and immediately after it are shown in Fig. 2. As follows from Fig. 2, the electron density changes slightly immediately after thermal quench, and the temperature in the center of the plasma decreases by approximately 2.5 times. The t_{CQ} value is ~0.7 ms in the discharge 42784.

Data on plasma current disruptions are shown in Figs. 3–6. The geometric parameters of the plasma were found using the algorithm of movable current rings [8, 9], which makes it possible to reconstruct the outermost closed magnetic surface of the plasma and magnetic surfaces beyond it. In the algorithm, the plasma current is replaced by a set of 19 movable rings. The input data are currents in the coils of the electromagnetic system, the plasma current and signals of the flux loops, located on the surface of the vacuum vessel. Examples of the reconstruction of the plasma boundary during the current quench are given in [1, 2].

Data obtained on the modernized Globus-M2 tokamak (circles in Figs. 3–6) refer to discharges with a toroidal magnetic field of 0.8–0.9 T, plasma elongation in the vertical direction of 1.7–1.9 before the disruption, and the average triangularity of the cross section of 0.25–0.33.

Figures 3 and 4 show the dependence of the current quench duration on the plasma current which generally confirms the regularity noted in [1]: an increase in $t_{CQ}(I_p)$ is close to the linear one. A weak dependence of the linear current decay rate I_p/t_{CQ} on the current density before the disruption is conserved (Fig. 5). A stronger difference is observed for the maximum current decay rate $dI_{p\max}/dt$, see Fig. 6. The plasma current dependence of the t_{CQ} value observed in our experiments is atypical for discharges in conventional tokamaks accumulated in the international experimental database on disruptions. This dependence, however, corresponds to the results obtained on the NSTX spherical tokamak [10].

In discharges at the Globus-M2 facility, a decrease in the hard X-ray HXR intensity of signals was systematically observed during the thermal and current

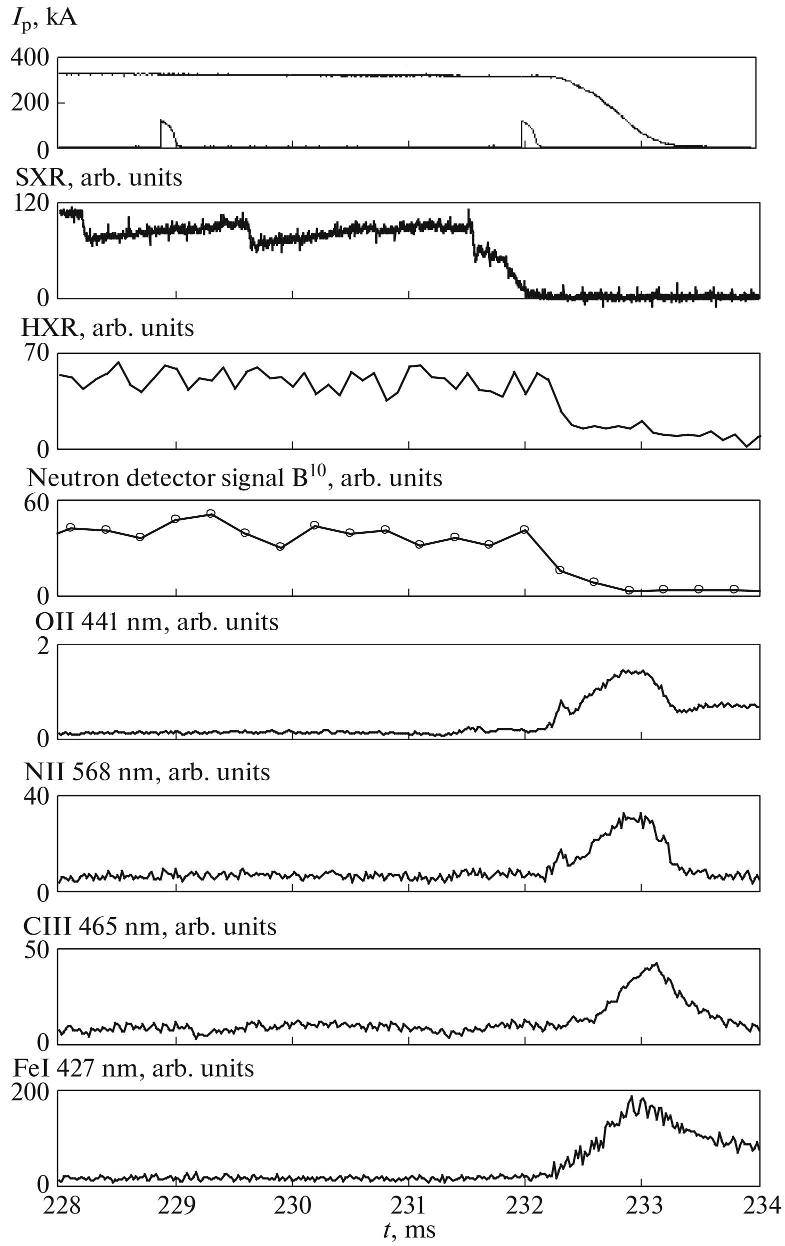

Fig. 1. Globus-M2, discharge 42784: evolution of plasma parameters during disruption. Top bottom: plasma current I_p and laser switching marks for Thomson scattering diagnostics (leading edge of the signal in the figure), soft X-ray SXR intensity, hard X-ray HXR intensity recorded by the detector $LaBr_3$, neutron detector signal B^{10}, emission intensity of OII, NII, CIII, and FeI lines. Plasma parameters before disruption: $B_{T0} = 0.8$ T, $\kappa = 1.96$, $\delta = 0.29$, $q_{95} = 6.6$.

quench. A typical dependence of the HXR evolution before and during disruption is shown in Fig. 1. It indicates the absence of any noticeable generation of runaway electrons during the disruption. It is noteworthy that the HXR intensity does not change after thermal quench. Its sharp decay begins only in the plasma current disruption phase.

Figure 1 also shows the emission dynamics of main impurity lines during the thermal and current quench. When interpreting these data, one should, generally speaking, take into account the displacement of the plasma during disruption in the vertical direction. Nevertheless, the data presented make it possible to draw a number of conclusions:

—The main input of impurities into the discharge occurs precisely during disruption; it is significantly less in the preceding discharge stage;

—an increase in the input of impurities into the plasma occurs already in the course of thermal quench

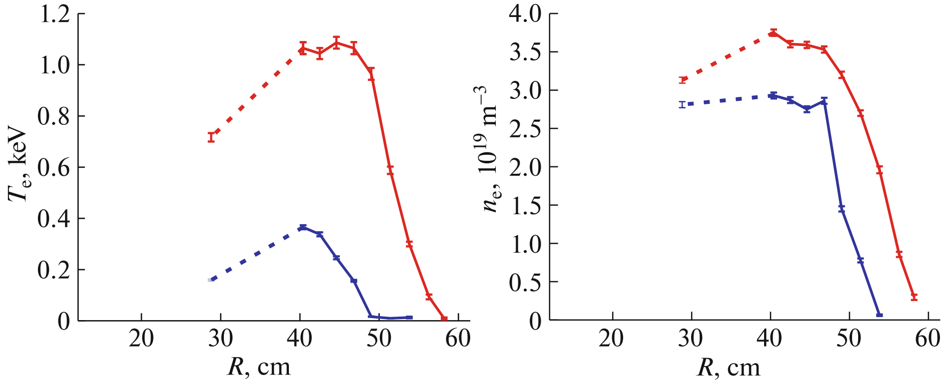

Fig. 2. Profiles of the electron temperature (left) and electron density (right) before thermal quench (red curves, $t = 229$ ms) and immediately after it (blue curves, $t = 232$ ms).

(see peaks in the emission intensity of the OII and NII lines in the discharge 42784 in Fig. 1); the emission intensity of the impurity lines continues to increase during the current quench period, which indicates their additional input.

In discharges, laser pulses of the Thomson scattering diagnostics for measuring the $n_e(r)$ and $T_e(r)$ profiles randomly get into different disruption stages. The discharge data in which the time of the measurement is displaced from thermal quench to the later current quench stage are given below. Despite the fact that these data were obtained in different discharges, they provide information on the evolution of the n_e and T_e profiles before and during the disruption, and on the input of impurities into the discharge (when comparing the $n_e(r)$ profile before and during the disruption).

In the discharge 42777 (Fig. 7), the laser pulse got into the very beginning of the current quench, when there was almost no vertical plasma escape, and the injection of atomic beams with a total power of about 800 kW terminated approximately 4 ms before the disruption.

Electron temperature and density profiles before the disruption and in the initial disruption stage are shown in Fig. 8. The electron temperature in the center of the plasma drops in approximately six times in the initial plasma disruption stage to a value of $T_e \sim$ 200 eV. The electron density in the center is half decreased. The flattening of the density profile is most likely due to the input of impurities from the walls into the discharge.

In the discharge 42145, T_e and n_e profiles were measured in the middle of the plasma disruption phase of the plasma. The position of the laser pulses is shown in Fig. 9. The same as in the discharge 42777 described above, the displacement of the plasma in the

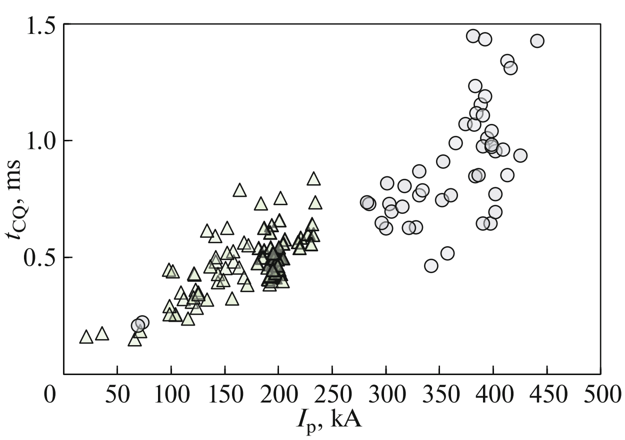

Fig. 3. Current decay time t_{CQ} as a function of the plasma current before the disruption. (△) Globus-M (data from [1]), (○) Globus-M2.

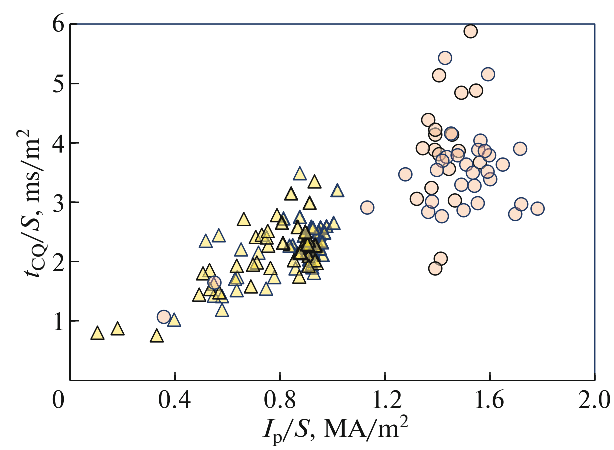

Fig. 4. Disruption time t_{CQ}/S normalized to the plasma cross-sectional area as a function of the plasma current density before the disruption. (△) Combined data for hydrogen and deuterium plasma in the Globus-M tokamak, (○) deuterium plasma, Globus-M2.

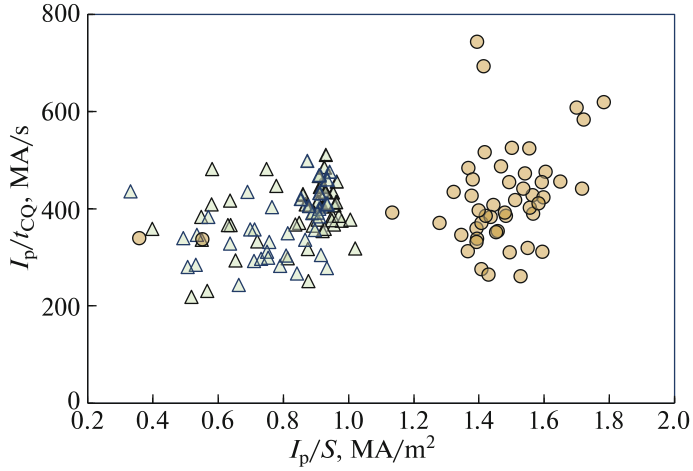

Fig. 5. Linear plasma current decay rate of during disruption depending on the current density before the disruption. (△) Globus-M data, (○) Globus-M2 data.

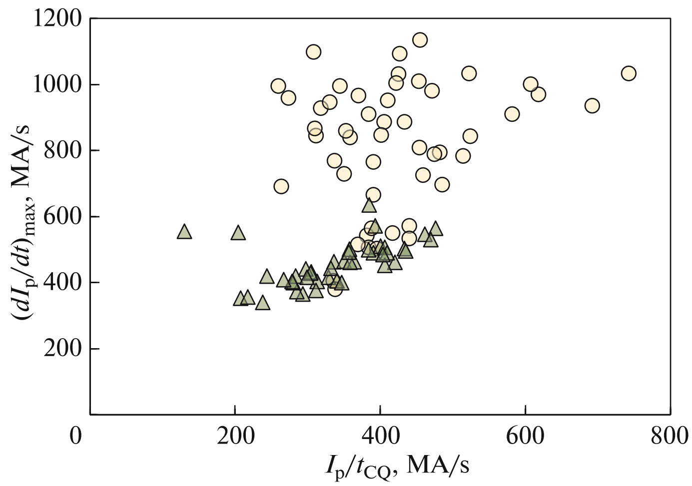

Fig. 6. Maximum rate of plasma current decay during disruption depending on the current density before the disruption. (△) Globus-M data, (○) Globus-M2 data.

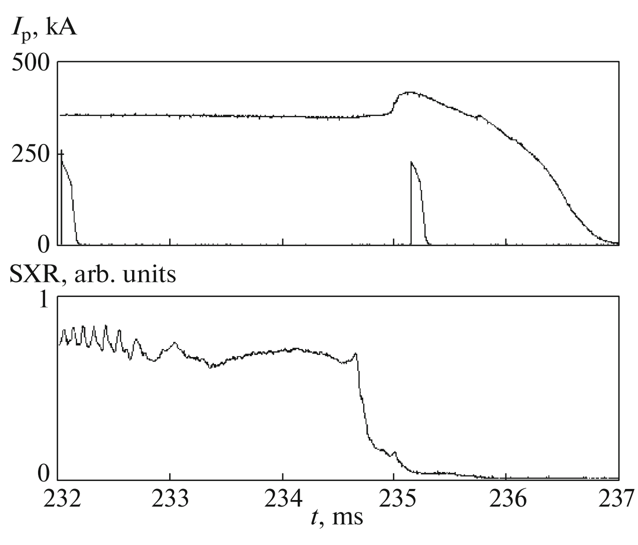

Fig. 7. Top bottom: I_p and laser pulses, SXR signal intensity in the discharge 42777. Plasma parameters before the disruption: $B_{T0} = 0.9$ T, $\kappa = 1.82$, $\delta = 0.29$, $q_{95} = 6.5$.

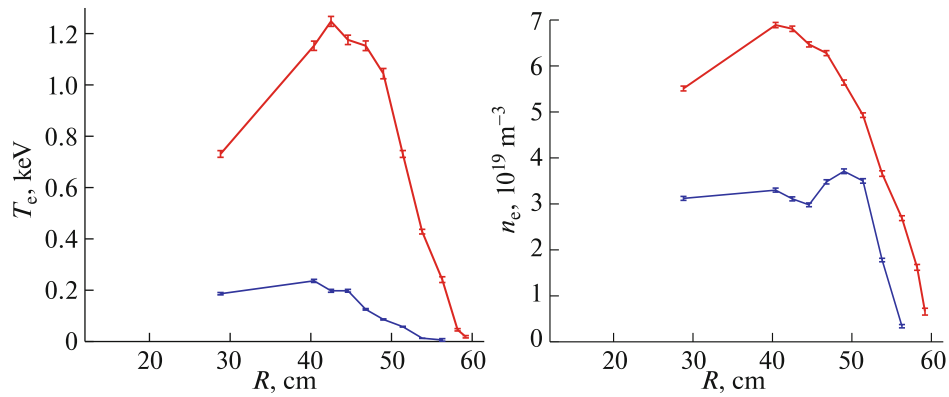

Fig. 8. Profiles of the electron temperature (left) and electron density (right) in the discharge 42777 before (red curves, $t = 232$ ms) and in the beginning of the plasma current quench (blue curves, $t = 235$ ms).

vertical direction at the time of measurements was slight. The disruption occurred during the injection of two beams with a total power of 1.6 MW.

Plasma electron temperature and density profiles are shown in Fig. 10. The temperature profile after the disruption is peaked. The density profile, on the contrary, has a maximum at the periphery. The electron density in the center of the plasma is approximately the same as before the disruption; it is twice as high at the periphery. A possible explanation for this density behavior is the input of impurities into the discharge. The fact that the temperature profile $T_e(r)$ is peaked may also be associated with the peripheral emission of impurities.

In general, the evolution of density and temperature profiles in the course of the current quench indicates the significance of the input of impurities from the walls.

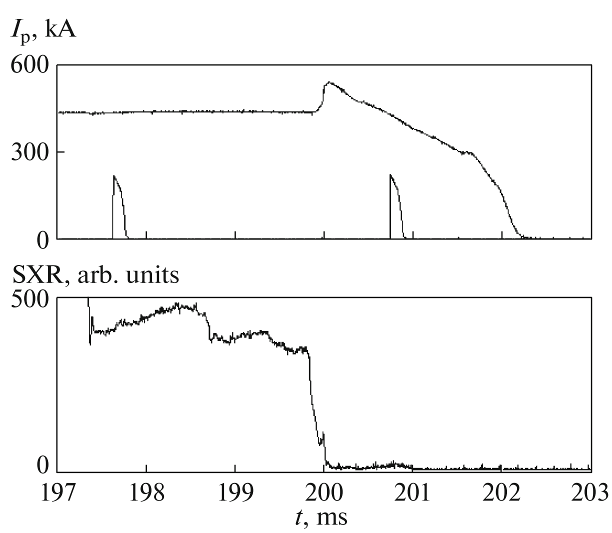

Fig. 9. Top down: I_p and laser switching marks, SXR signal intensity in the discharge 42145. Plasma parameters before the disruption: $B_{T0} = 0.8$ T, $\kappa = 1.89$, $\delta = 0.34$, $q_{95} = 6.4$.

3. HEATING OF THE PLASMA-FACING SURFACE DURING DISRUPTION

An infrared camera [9] mounted in the equatorial plane of the tokamak was used to study the heating of the plasma-facing surface. The main surface of the vessel is covered with graphite tiles. The measurements were carried out in a 64 × 52 pixel window with a frame rate of 2.6 kHz. Figure 11 shows the temperature of a graphite plate located in the middle plane of the torus from the low-magnetic-field side during the disruption in the discharge 42363 and the calculated thermal flux: on the left (region *2* in Fig. 12a) and on the right (region *3* in Fig. 12a). Two beams with a total power of 1.1 MW were injected into the plasma during the disruption.

The heating of the plate on the left is determined mainly by plasma ions, while that on the right is determined by electrons. Because of the inaccurate mounting, this plate and the plate above it are moved a few millimeters closer to the center of the tokamak. Therefore, the plates on the right are in their shade. Figure 12b shows the temperature distribution of the surface of the plates (region 1 in Fig. 12a) immediately after thermal quench and after the start of the plasma disruption (approximately 1 ms after the start of thermal quench). Thermal imager data indicate that the plate is heated by ions during thermal quench. Electron heating is divided into two stages: the first part of electrons is lost during thermal quench, and the second part is lost during the plasma disruption, which does not contradict the data of Thomson scattering diagnostics. We also note that the heating of the wall is local and does not exceed 100°C, and the thermal flux is not higher than 9 MW/m^2, which is comparable to the heating of the wall caused by sawtooth oscillations.

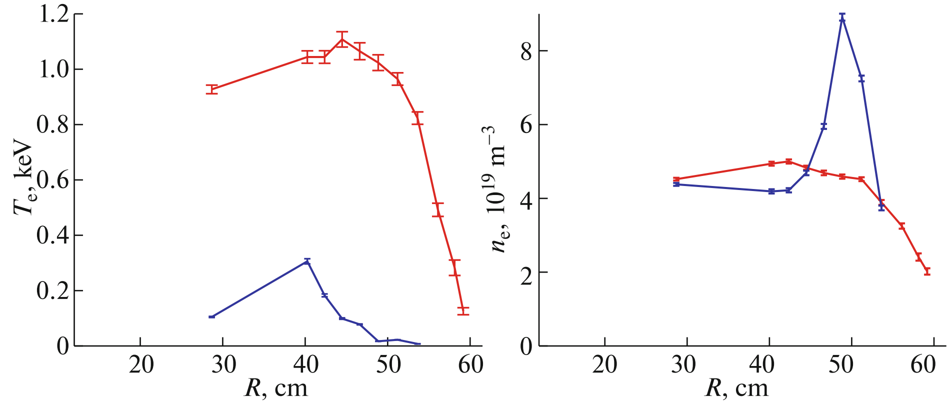

Fig. 10. Profiles of the electron temperature (left) and electron density (right) in the discharge 42145 before (red curves, t = 198 ms) and in the middle of the phase (blue curves, t = 201 ms) of the plasma current quench.

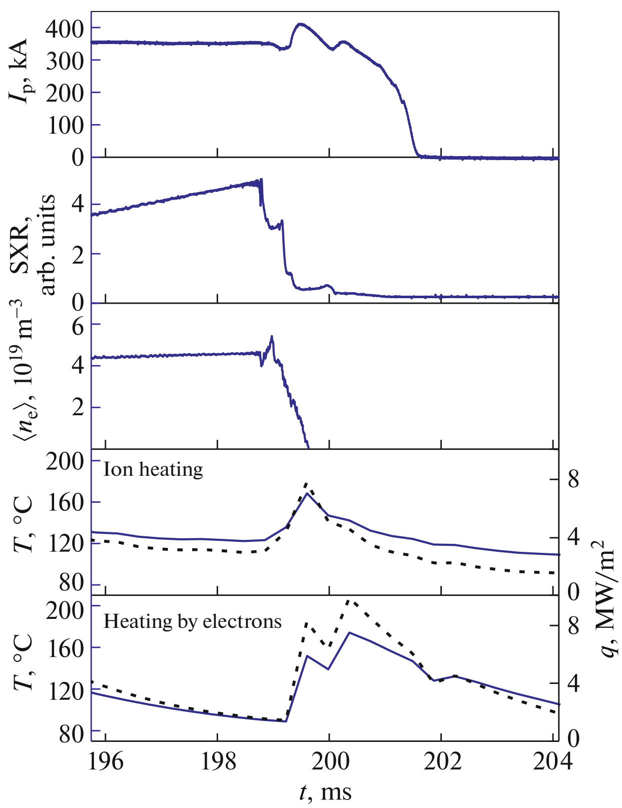

Fig. 11. Globus-M2, discharge 42363: evolution of parameters during the disruption in the discharge 42263. Top down: plasma current I_p, soft X-ray radiation SXR intensity, average density along the observation chord $\langle n_e \rangle$, graphite plate surface temperature (solid line) and thermal flux (dotted line) in the regions *2* (ion heating) and *3* (electron heating) in Fig. 12a. Plasma parameters before the disruption: $B_T = 0.9$ T, $\kappa = 1.75$, $\delta = 0.34$, $q_{95} = 7.9$.

4. ELECTROMAGNETIC LOADS ON THE TOKAMAK VESSEL DURING PLASMA DISRUPTION

The discharge 42 145 with a plasma current before the disruption of 440 kA in a toroidal magnetic field of 0.8 T was chosen for the analysis of electromagnetic loads on the vessel. Figure 13 shows the evolution of the plasma current and the total induced toroidal current in the vacuum vessel. The plasma was shifted towards the lower dome during the disruption. The design of the steel shell of the vessel is described in [2]. It is important to note that the maximum induced cur-

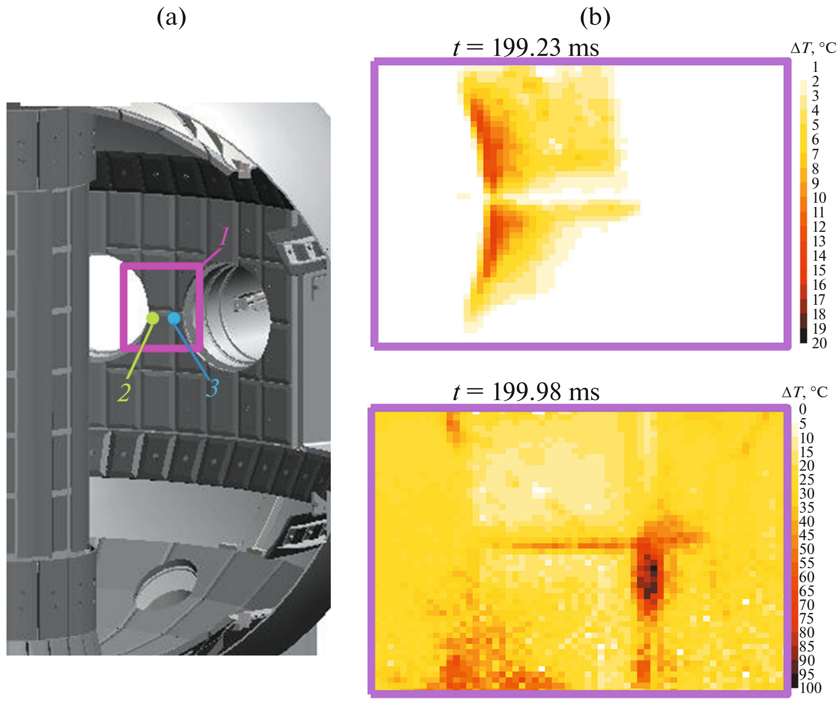

Fig. 12. (a) Tokamak vessel, inside view. (*1*) Observation region of the thermal imager. Regions *2* and *3* correspond to heating of the graphite plate by ions and electrons, respectively. (b) Discharge 42363, heating of the plates in the region *1* in 0.38 ms after the start of thermal quench (top) and in 1.14 ms after thermal quench (bottom).

rent is "only" 160 kA at the pre-disruption plasma current of ~440 kA, which is significantly less than the expected values based on the results of experiments in a low toroidal magnetic field $B_T = 0.25–0.5$ T on the Globus-M tokamak [2]. In our opinion, this is a consequence of an increase in the current quench duration with an increase in the plasma current (see Fig. 3).

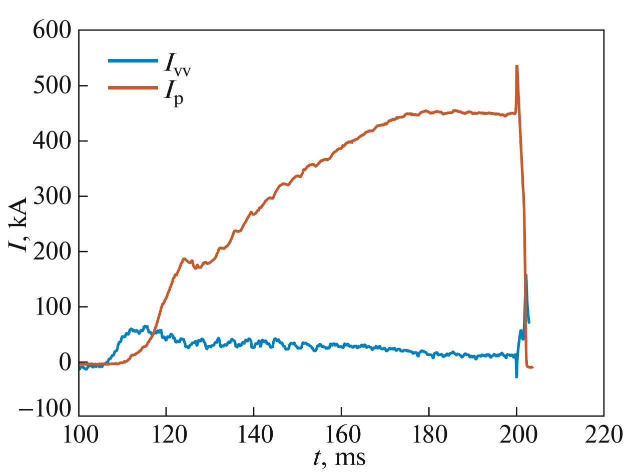

Fig. 13. Evolution of the plasma current I_p and total toroidal current over the vessel I_{vv} in the discharge 42 145.

The distribution of the maximum current induced into the vessel over the poloidal direction of the vacuum vessel during the disruption ($t \approx 202.3$, $I_{vv} \approx 160$ kA) is shown in Fig. 14. The maximum current value is achieved near the middle plane of the torus from the low- and high-magnetic-field side.

Figure 15a shows the distribution of the normal electromagnetic pressure on the vessel P_n at the time $t \approx 202.3$ ms. The pressure value is calculated as the product of the toroidal current induced in the elements of the vessel by the poloidal magnetic field tangent to the surface of the vessel. The positive normal pressure values correspond to the direction outward from the vessel circuit. As an illustration, Fig. 15b shows the normal pressure on the vessel by arrows. The direction of the arrows corresponds to the pressure direction, and their length is proportional to its magnitude. The maximum absolute pressure value on the vessel is ≈35 kPa.

5. DISCUSSION OF RESULTS

The data of the study of the large plasma current quench at the Globus-M2 tokamak described in this work confirm the main conclusions made in [1, 2] based on the results of experiments on the Globus-M tokamak under conditions of approximately 2–3 times lower toroidal magnetic field and plasma current. The favorable linear dependence of the disruption time on

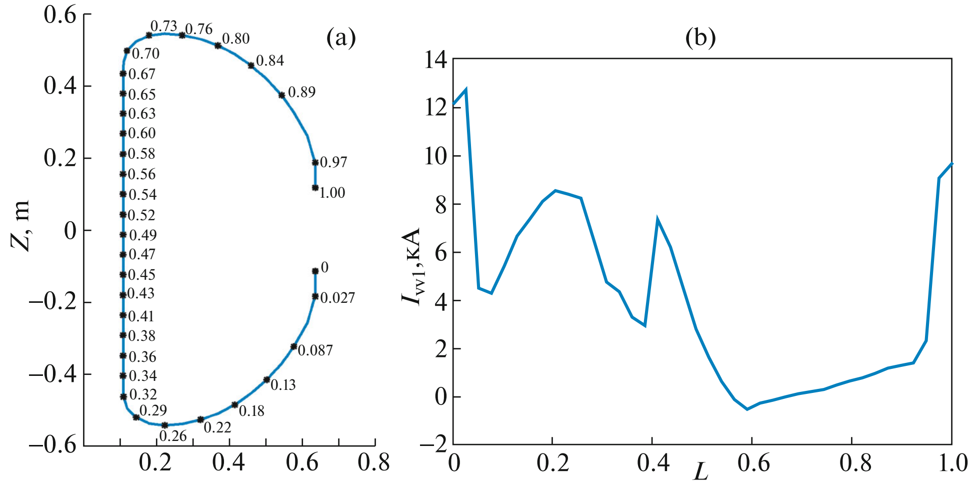

Fig. 14. (a) Cross section of the vacuum vessel with the indication of the poloidal length reference in relative units (current length l divided by the total length of the perimeter minus the 400 mm diameter pipes in the outer ring); (b) distribution of induced toroidal current vessel I_{vv1} over the poloidal length in the discharge 42145 at time $t \approx 202.3$ ms (maximum current at disruption $I_{vv} \approx 160$ kA).

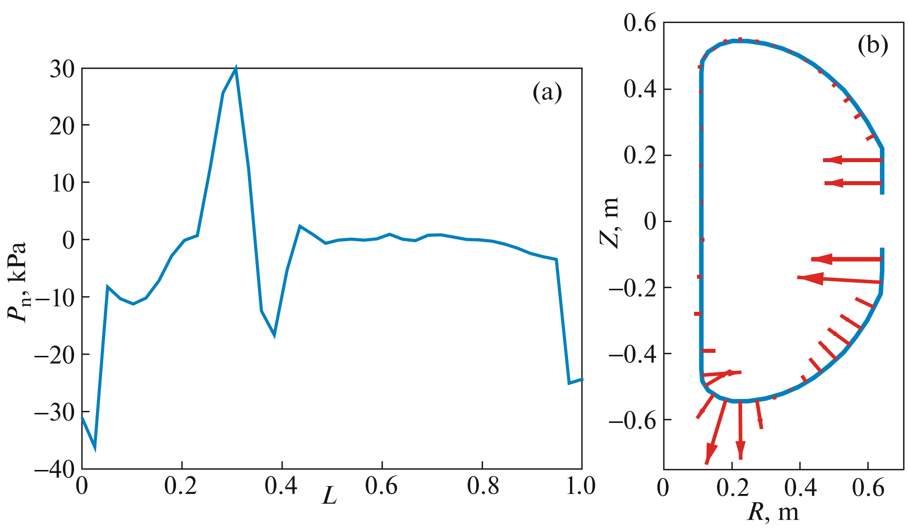

Fig. 15. (a) Distribution of the normal pressure on the vessel along the poloidal length in the discharge 42145 at time $t \approx 202.3$ ms; (b) diagram of the distribution of the normal pressure over the vessel at time $t \approx 202.3$ ms.

the pre-disruption plasma current, characteristic for a spherical tokamak, was preserved. The toroidal current in the vessel induced at the disruption was somewhat less than expected according to [2], which led to a decrease in the electrodynamic loads acting on the vessel. The modernized diagnostics of Thomson scattering of laser radiation made it possible to measure the electron temperature and density profiles in ten spatial points immediately after thermal quench and at different times during the current quench phase. Based on systematic measurements of the hard X-ray radiation intensity, the conclusion was confirmed that there is no noticeable generation of runaway electrons at the disruption.

The accumulated information on disruptions can be used to extrapolate the characteristics of disruption to the parameters of the Globus-3 tokamak, which is currently in the pre-design stage. The preliminary basic parameters for the Globus-3 facility are: R = 0.76 m, a = 0.44 m, $\kappa \sim 1.8$, I_p = 800 kA, and B_{T0} = 1.5 T. For the specified parameters, the plasma cross section before the disruption $S \approx 1$ m^2, and the plasma current density $j_p = I_p/S \approx 0.8$ MA/m^2. In this case, the parameters are in the middle part of Fig. 4, and the estimate of the current quench time in the Globus-3 gives $t_{CQ}/S \sim 2.5$ ms/m^2 and $t_{CQ} \sim 3$ ms. In this case, we obtain a relatively small value $I_p/t_{CQ} \approx 200$–300 MA/s for the average current decay rate, which makes it possible to count on moderate electrodynamic loads on the vessel.

ACKNOWLEDGMENTS

The study was carried out on the unique Spherical Globus-M scientific tokamak facility, which is a part of the Federal Center for Collective Use of the Ioffe Physical Technical Institute, Russian Academy of Sciences "Materials Science and Diagnostics in Advanced Technologies."

FUNDING

The preparation of experiments and auxiliary plasma heating sources was supported by the State assignment (themes 0040-2019-0023 and 0034-2021-0001). Experimental results and calculations given in Sections 2–8 were supported of the Russian Science Foundation (project no. 21-79-20133 of March 24, 2021).

CONFLICT OF INTEREST

The authors of this work declare that they have no conflicts of interest.

REFERENCES

1. N. V. Sakharov, V. K. Gusev, A. D. Iblyaminova, A. A. Kavin, S. N. Kamenshchikov, G. S. Kurskiev, K. M. Lobanov, V. B. Minaev, A. B. Mineev, M. I. Patrov, Yu. V. Petrov, and S. Yu. Tolstyakov, Plasma Phys. Rep. **43**, 422 (2017).
2. N. V. Sakharov, V. K. Gusev, A. A. Kavin, S. N. Kamenshchikov, K. M. Lobanov, A. B. Mineev, M. I. Patrov, and Yu. V. Petrov, Plasma Phys. Rep. **44**, 387 (2018).
3. ITER Physics Basis, ITER Physics Expert Group Chairs and Co-Chairs, and ITER Joint Central Team and Physics Integration Unit, Nucl. Fusion **39**, 2137 (1999).
4. N. W. Eidietis, S. P. Gerhardt, R. S. Granetz, Y. Kawano, M. Lehnen, G. Pautasso, V. Riccardo, R. L. Tanna, A. J. Thornton, and the ITPA Disruption Database Participants, Nucl. Fusion **55**, 063030 (2015).
5. A. B. Mineev, E. N. Bondarchuk, A. A. Kavin, A. Yu. Konin, I. Yu. Rodin, V. N. Tanchuk, O. G. Filatov, N. N. Bakharev, N. S. Zhilzov, G. S. Kurskiev, E. O. Kiselev, V. B. Minaev, N. V. Sakharov, Yu. V. Petrov, and A. Yu. Telnova, Phys. At. Nucl. **85**, 1194 (2022).
6. A. B. Mineev, E. N. Bondarchuk, A. A. Kavin, A. Yu. Konin, I. Yu. Rodin, V. N. Tanchuk, V. A. Trofimov, O. G. Filatov, N. N. Bakharev, N. S. Zhilzov, G. S. Kurskiev, E. O. Kiselev, V. B. Minaev, N. V. Sakharov, Yu. V. Petrov, et al., Phys. At. Nucl. **85**, 1205 (2022).
7. A. B. Mineev, V. B. Minaev, N. V. Sakharov, N. N. Bakharev, E. N. Bondarchuk, A. A. Voronova, A. M. Glushaev, S. A. Grigoriev, V. K. Gusev, N. S. Zhiltsov, E. R. Zapretilina, A. A. Kavin, E. O. Kiselev, A. Yu. Konin, A. M. Kudriavtseva, et al., Phys. At. Nucl. **85** (Suppl. 1), S17 (2022). https://doi.org/10.1134/S1063778822130099
8. V. I. Vasiliev, Yu. A. Kostsov, K. M. Lobanov, L. P. Makarova, A. B. Mineev, V. K. Gusev, R. G. Levin, Yu. V. Petrov, and N. V. Sakharov, Nucl. Fusion **46**, S625 (2006).
9. N. V. Sakharov, A. V. Voronin, V. K. Gusev, A. A. Kavin, S. N. Kamenshchikov, K. M. Lobanov, V. B. Minaev, A. N. Novokhatskii, M. I. Patrov, Yu. V. Petrov, and P. B. Shchegolev, Plasma Phys. Rep. **41**, 997 (2015).
10. S. P. Gerhardt, J. E. Menard, and the NSTX Team, Nucl. Fusion **49**, 025005 (2009).

Translated by L. Mosina